
**Liquid Crystals**
Publication details, including instructions for authors and subscription information:
http://www.informaworld.com/smpp/title~content=t713926090

# A technique for measurement of pretilt angles arising from alignment layers

Marie-Pierre Cuminal; Monique Brunet

Online publication date: 06 August 2010

**To cite this Article** Cuminal, Marie-Pierre and Brunet, Monique(1997) 'A technique for measurement of pretilt angles arising from alignment layers', Liquid Crystals, 22: 2, 185 — 192
**To link to this Article: DOI:** 10.1080/026782997209559
**URL:** http://dx.doi.org/10.1080/026782997209559

LIQUID CRYSTALS, 1997, VOL. 22, NO. 2, 185–192

# A technique for measurement of pretilt angles arising from alignment layers

by MARIE-PIERRE CUMINAL and MONIQUE BRUNET*

Groupe de Dynamique des Phases Condensées, Université Montpellier II C.C.26, F-34 095 Montpellier Cedex 05, France

(*Received 19 July 1996; accepted 1 October 1996*)

A well-controlled, reproducible alignment with or without a pretilt angle is a basic need for the development of any kind of liquid crystal display. We have built an optical set-up based on the crystal rotation method. With this system we can measure the pretilt angle in non-twisted liquid crystal samples. Presentation of the experimental set-up and first results of these measurements (obtained with a precision of 0·3°) are given for several compounds and alignment layers.



## 1. Introduction

Liquid crystals are materials possessing a long range orientational order which can be improved and controlled by specific treatments of anchoring surfaces. Because of their fluidity, liquid crystals have to be confined between two glass plates to form a cell. These plates are coated with a thin orientation layer which induces a molecular alignment and a preferential orientation on the surfaces and in all the sample, if it is not too thick. There are different types of alignment depending on the material and the deposition technique chosen. In the homeotropic alignment the molecules lie perpendicular to the surface plane, whereas in the planar one the molecules lie in the plane of the substrate, and in the tilted orientation the molecules make an angle $\alpha$ with the cell surfaces. This angle, called the 'pretilt angle', strongly influences the performance of liquid crystal devices such as displays used for industrial applications. It is very important, at present, to measure pretilt angles with a high reproducibility and accuracy to understand and investigate anchoring effects in confined liquid crystals. Several methods exist [1–5] to measure this angle, with their own performances and disadvantages, as well as two industrial versions (ELDIM, AUTRONIC) [6]. It is quite difficult to compare all these experimental techniques and results because of the different measurement conditions.

We have chosen the classical crystal rotation method previously described by Baur *et al.* [7] and also by Scheffer and Nehring [8] to build an experimental optical set-up which can measure the pretilt angle $\alpha$, in non-twisted liquid crystal cells, with a precision of 0·3°. The main advantage of our measurement method is that it gives the pretilt angle with the same precision in cells with different thicknesses. In this paper, we detail our experimental set-up and present the first results obtained at room temperature with several liquid crystal compounds aligned by different layers.

*Author for correspondence.

## 2. Crystal rotation method

### 2.1. *Theoretical model*

The liquid crystal is confined between two parallel glass plates, coated with a thin alignment layer whose unique directions are antiparallel. The director **n** is supposed to have a homogeneous distribution throughout the whole cell, so it forms a uniaxial single crystal, the optical axis of which makes an angle $\alpha$, supposed constant throughout the liquid crystal cell, with the plane of the substrates. The principle of the crystal rotation method is to measure the optical transmission of the cell between two crossed polarizers, oriented at 45° from the incident plane, as a function of the incident light angle $\Psi$ (figure 1). The cell is rotated around an axis which is perpendicular to the optical axis of the liquid crystal.

In this system, the phase difference between the ordinary and extraordinary optic modes is given by:

$$\varphi = \frac{2\pi d}{\lambda} f(\alpha, \psi) = \frac{2\pi\delta}{\lambda} \qquad (1)$$

where $d$ is the cell thickness, $\lambda$ is the wavelength of the incident light, $\delta$ is the cell optical retardation and $f(\alpha, \Psi)$ is a birefringence function, depending on $\alpha$ and $\Psi$, expressed by Françon [9] as:

0267–8292/97 $12·00 

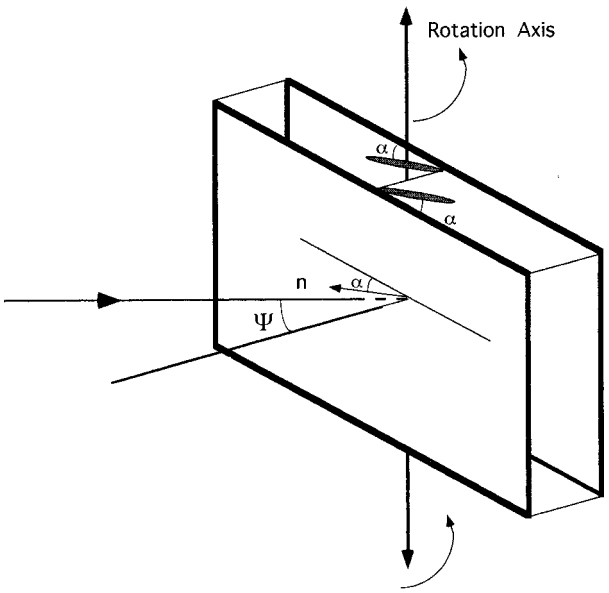


Figure 1. A liquid crystal cell of thickness $d$; $\alpha$ is the pretilt angle, $\Psi$ is the incident light angle, $\lambda$ is the light wavelength and **n** is the director of the liquid crystal.

$$f(\alpha, \psi) = \frac{n_o^2 - n_e^2}{n^2} \sin\alpha \cos\alpha \sin\psi + \frac{n_o n_e}{n^2} (n^2 - \sin^2\psi)^{1/2} - (n_o^2 - \sin^2\psi)^{1/2}$$

$$\text{with} \quad n^2 = n_o^2 \cos^2\alpha + n_e^2 \sin^2\alpha \tag{2}$$

Here $n_o$ and $n_e$ are the ordinary and extraordinary refractive indices of the liquid crystal; $n_e$ is parallel to the liquid crystal director **n** whereas $n_o$ is perpendicular to $n$. The light transmission through this uniaxial section and with the conditions defined above is given by:

$$T = \sin^2\left[\frac{\pi d}{\lambda} f(\alpha, \psi)\right] \tag{3}$$

The function $T(\Psi)$ is almost symmetrical around a particular angle $\Psi_x$ corresponding to an extreme value of the optical retardation $\delta$ (such a curve is shown in figure 2 *(a)*) which corresponds to:

$$\left(\frac{d\delta}{d\psi}\right)_{\psi=\psi_x} = 0 \tag{4}$$

and so:

$$\left(\frac{df}{d\psi}\right)_{\psi=\psi_x} = 0 \tag{5}$$

After derivation we obtain the relation:

$$\left[(n_o^2 - \sin^2\psi_x)^{-1/2} - \frac{n_o n_e}{n^2}(n^2 - \sin^2\psi_x)^{-1/2}\right] \sin\psi_x = \frac{n_e^2 - n_o^2}{n^2} \sin\alpha\cos\alpha \tag{6}$$

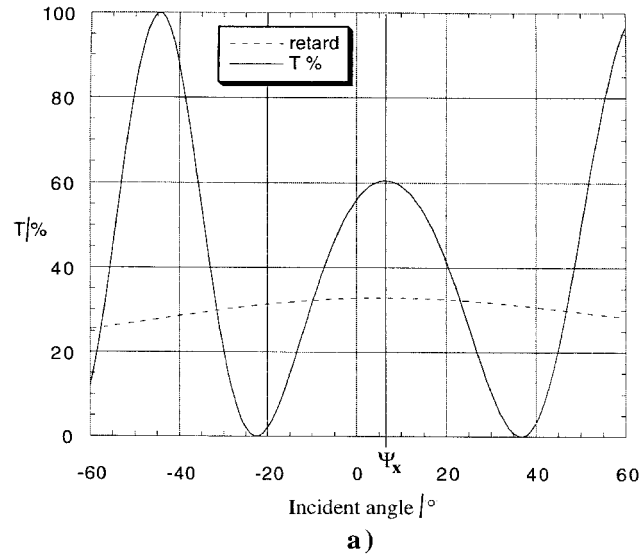


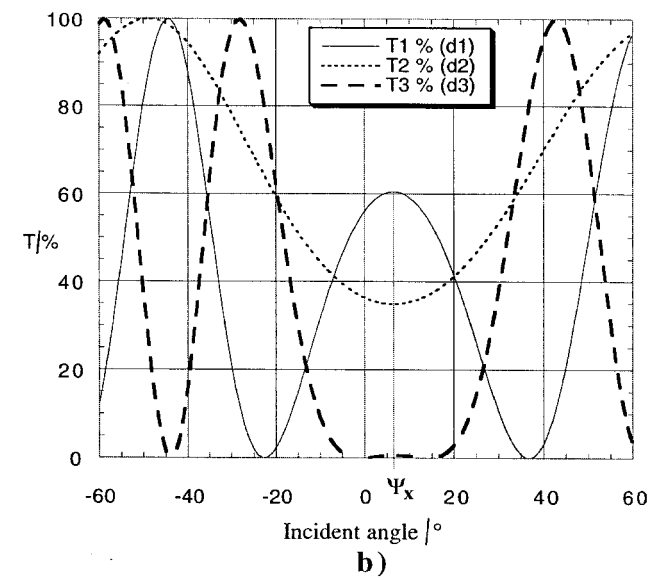


Figure 2. Theoretical angular dependence of transmission $T$ and optical retardation $\delta$ as a function of incident angle $\Psi$ for a nematic cell (ZLI-3219) with $\lambda = 589$ nm, $n_e = 1{\cdot}7188$, $n_o = 1{\cdot}5138$ and $\alpha = 2°$. *(a)* $d = 15\,\mu$m; the particular angle $\Psi_x$ on the $T$ curve corresponds to the maximum of the $\delta$ curve. *(b)* $d = 15\,\mu$m for $T1$, $d = 5\,\mu$m for $T2$, $d = 20\,\mu$m for $T3$. The form of the $T$ curve changes, but not the position of the extremum $\Psi_x$.

$\Psi_x$ can be determined graphically and so $\alpha$ can be calculated, knowing the values of the extraordinary and ordinary refractive indices $n_e$ and $n_o$ and using the relation (6). Notice that the calculation of $\alpha$ is dependent only on the liquid crystal refractive indices $n_e$ and $n_o$ and independent of the thickness $d$ and the wavelength $\lambda$ (although the refractive indices do depend on $\lambda$). Figure 2 *(b)* shows theoretical transmission curves for a nematic cell with different thickness values. The form of

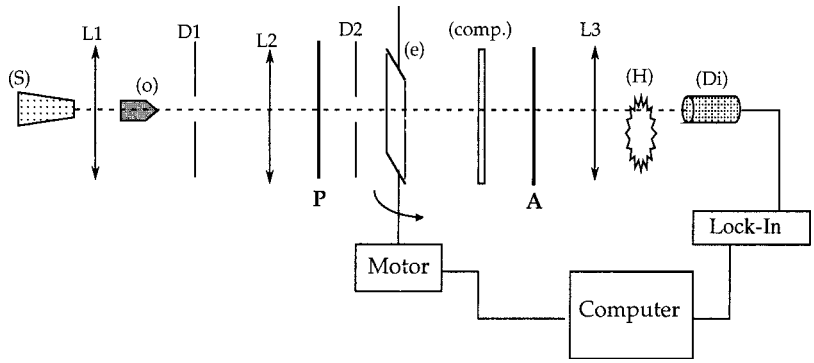


Figure 3. Scheme of the experimental optical set-up: (S) is the white light source, (e) the LC sample, (o) the objective, (H) the chopper, (Di) the detection diode, (comp.) the compensator; L1, L2, L3 are the lenses, D1 and D2 are the diaphragms, **P** represents the polarizer and **A** the analyser.

the $T(\Psi)$ curve changes, but not the position of the extremum $\Psi_x$.

### 2.2. *The optical set-up*

Figure 3 represents the optical set-up we have built. We use white light (100 W, 12 V) in order to have higher intensities, after verification by experimental measurements that the impact of the small variations in the refractive indices with wavelength can be neglected in comparison with the precision obtained. Figure 4 shows an example of the transmission for the same nematic cell measured with the white light *(a)* and with a monochromatic filter $\lambda = 600 \pm 50$ nm *(b)*. We can observe that the position of the extremum $\Psi_x$ is not changed and so the pretilt angles calculated are the same. Using the filter, we had to change the sensitivity of the lock-in amplifier, because the detected intensity was smaller. This is probably why the transmission curve shown in figure 4 shows more noise.

The theory is available for a parallel light beam passing through the liquid crystal cell. To obtain a quasi-parallel beam, we use a microscope objective Leitz UT40, a 200 μm diameter diaphragm and a biconvex lens with a focal length of 100 mm. The actual estimated deviation is about $10^{-3}$ rad. The second diaphragm has a variable diameter and is used to choose the measured area in the cell from 2 to 6 $mm^2$. Polarizer and analyser are crossed and oriented at 45° to the cell's principal plane defined by the normal to the plates and the unique direction **n**. The sample is rotated with a Micro-Controle step by step motor (IT6D CA1) around an axis which is perpendicular to the optical axis of the liquid crystal. The role of the Soleil–Bravais compensator is to change the detected optical retardation, which means in our conditions to add a phase. So, by choosing the best compensation, it is possible to obtain the most favourable transmission curve $T(\Psi)$ and thus the best graphical determination of the angle $\Psi_x$ for any cell thickness. Figure 5 shows two transmission curves, *(a)* obtained without compensation and *(b)* chosen for a good compensation, so that the determination of $\Psi_x$ is easier and more precise in the case of curve *(b)*. Thus, the compensator allows the same measurement precision for arbitrary sample thickness. Figure 6 shows the transmission curves for one cell with different compensation values. The lens 3 focuses the light beam on the photodiode PIN. A 1 Ω resistance is connected in series with the photodiode to assure a linear response. The signal is then detected by the lock-in amplifier (SR830 Stanford Research) with the frequency chopper (SR540 Stanford Research) reference (1200 Hz). Since all these optical elements have been chosen, positioned and adjusted with great care and precision, we have obtained an accurate determination of $\Psi_x$ and so a precision of $\pm 0{\cdot}3°$ for the pretilt angle $\alpha$. The set-up has been fully automated with a LabVIEW program specially conceived to drive the motor and the lock-in amplifier and also to collect the data.

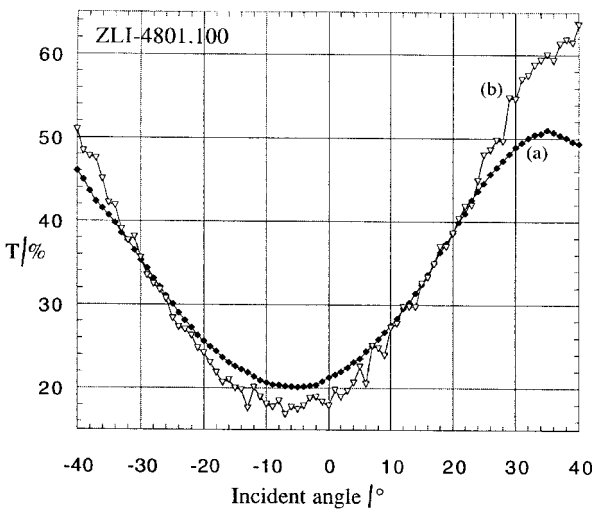


Figure 4. Measured transmission $T$ for a cell with the nematic (ZLI-4801.100, $d = 14$ μm) on a polyimide layer deposited by THOMSON-LCD; *(a)* white light, *(b)* $\lambda = 600 \pm 50$ nm. For both curves $\Psi_x = 4{\cdot}5°$, so $\alpha = 1{\cdot}5°$.

### 2.3. *Oblique reflections*

The error induced by oblique reflections between interfaces, air/glass and glass/liquid crystal, for both cell

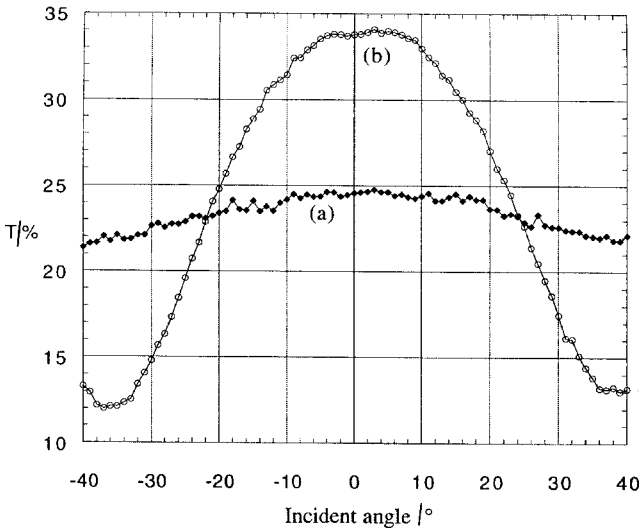


Figure 5. Measured transmission $T$ as a function of incident angle $\Psi$ for the nematic liquid crystal ZLI-3219, $d = 13\,\mu m$, on a PTFE layer. Curve *(a)* shows results obtained without the compensator; curve *(b)* is obtained choosing the compensation value best adapted to determine $\Psi_x$ with the greatest precision.

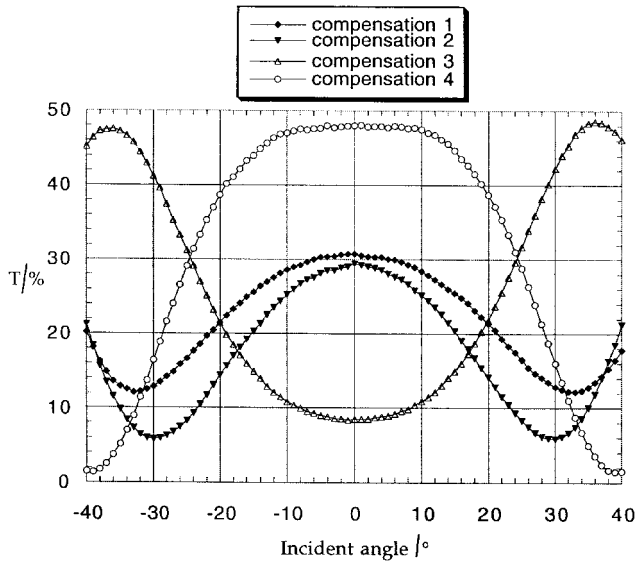


Figure 6. Measured transmission $T$ for a nematic cell (ZLI-3219) with different values of the compensation; $\Psi_x$ is always the same at about 0·5°.

surfaces has been estimated. The surface reflection factor is defined as the ratio between the reflected and transmitted intensities of light. For a normal reflection between a first medium of refractive index $n_1$ and a second medium of refractive index $n_2$, the reflection factor is given by the relation:

$$R = \left(\frac{n-1}{n+1}\right)^2$$

where $n$ is the ratio $n_2/n_1$. In the case of the media glass/liquid crystal, the coefficient $n$ is around 1·1, so the reflection factor is $R \approx 0{\cdot}002$, which means about 4% of the total energy reflected by both interfaces; this can be considered as negligible. Concerning the reflection between the media air/glass, the coefficient $n$ is around 1·5 and $R \approx 0{\cdot}004$, giving 8% of reflected energy for both cell plates. But this reflection factor changes when the incident light angle changes. We know the Fresnel coefficients [10] $R_\parallel$ and $R_\perp$ for vibrations parallel or perpendicular to the wave plane:

$$R_\parallel = \left[\frac{\tan(\theta_i - \theta_t)}{\tan(\theta_i + \theta_t)}\right]^2 \quad R_\perp = \left[\frac{\sin(\theta_i - \theta_t)}{\sin(\theta_i + \theta_t)}\right]^2$$

where $\theta_i$ and $\theta_t$ are the incident and transmission angles. In the case of our optical set-up, the polarization direction makes an angle of 45° with the wave plane and the incident angle varies from 0° to 40°. This is the most favourable case for minimization of the reflected energy. We have estimated the reflection factor $R'$ in our case as:

$$R' = \frac{1}{2}(R_\parallel + R_\perp)$$

The graphical representation of $R'$ as a function of the angle of incidence (figure 7) shows small variations of this factor between 0° and 40°. Calculations also show a very small influence of these reflections on the experimental results. In fact we can observe that taking these oblique reflections into account in the theoretical model changes the amplitude of the transmission curve, but never changes the determined $\Psi_x$ value (figure 8). Nevertheless we decided to take them into account, and so all the data have been corrected before being plotted.

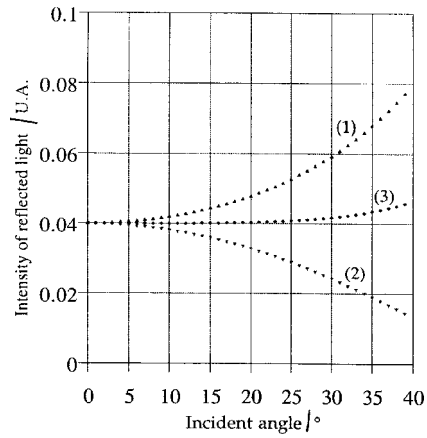


Figure 7. Intensity of reflected light as a function of the angle of incidence: (1) $R_\parallel$, (2) $R_\perp$, (3) $R' = \frac{1}{2}(R_\parallel + R_\perp)$.

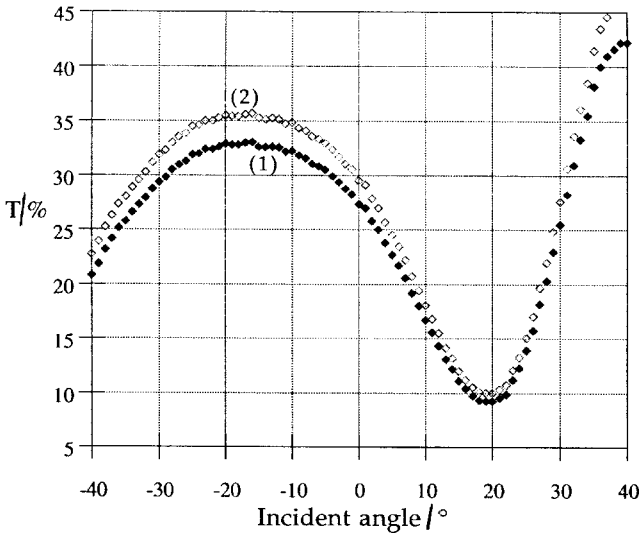


Figure 8. Curve (1) represents the measured transmission $T$ as a function of incident angle for a nematic cell with $d = 14{\cdot}5\,\mu m$; liquid crystal ZLI-3219 on polyimide deposited by THOMSON-LCD. Curve (2) represents the same transmission with the corrections induced by oblique reflections.

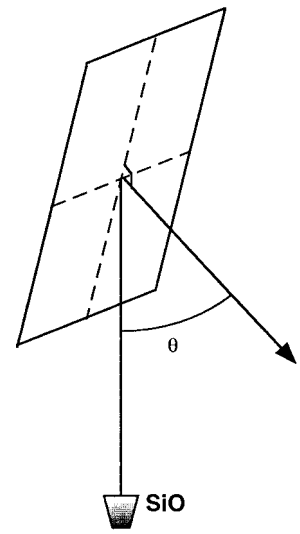


Figure 9. Position of the glass substrate used for oblique deposition; the angle $\theta$ used can be 60° or 80°.



### 3. Experimental conditions

The samples used are liquid crystal cells prepared with two glass plates from Balzers with a thin ITO (Indium Tin Oxide) layer. These glass plates are 1·1 mm thick and $2 \times 3\,cm^2$ size. These are carefully cleaned, dried and coated with a thin aligning layer. This layer induces a preferential molecular alignment on the surfaces and in all the cell if it is not too thick. We have used different types of orientation layers:

— oblique evaporation of SiO [11, 12] at 60° or 80° (figure 9) with the normal to the substrate;
— oblique sputtering [13] of SiO in argon plasma and at 60° or 80° with the normal to the substrate (figure 9);
— mechanical deposition of a thin layer of poly-(tetrafluoroethylene) (PTFE) at controlled temperature, rate and pressure, according to the Wittmann method [14];
— polyimide layer deposited by THOMSON-LCD.

Cells are made with two parallel plates, spaced with four mylar spaces 12 μm thick and glued with Norland UV91. The cell gap is then measured with a spectrometer, measuring interference fringes, before being filled with a liquid crystal in the isotropic phase. We have used different liquid crystal materials from E. Merck, nematic at room temperature, with different birefringence values: ZLI-3219 with $\Delta n = 0{\cdot}2050$, ZLI-4389 with $\Delta n = 0{\cdot}1567$, ZLI = 4518 with $\Delta n = 0{\cdot}0712$, ZLI-4801.100 with $\Delta n = 0{\cdot}1055$ and ZLI-5080 with $\Delta n = 0{\cdot}0865$. We also used materials in the smectic A phase at room temperature: K24 and S3 from Merck Ltd.

### 4. Experimental results

Experiments have been coupled with numerical calculations as described above. Measurements show a good reproducibility and precision as shown in figure 10. The table presents some of the results we obtained at room temperature (~25°C), with several compounds on different layers, and with a precision of ±0·3°.

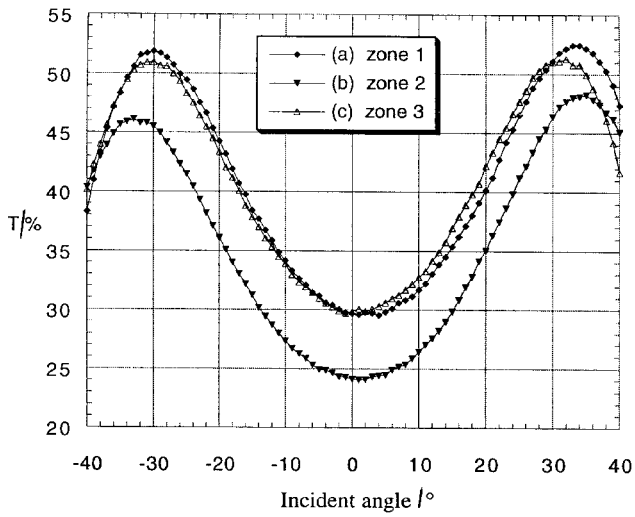


Figure 10. Measured transmission $T$ as a function of the incident angle $\Psi$ for a nematic cell with $d = 13{\cdot}5\,\mu m$; liquid crystal ZLI-3219 on 1000 Å of SiO evaporated at 60°. Measurements were made in three different regions of the cell; $\Psi_x = 0{\cdot}8°$, $\alpha = 0{\cdot}3°$.

Table. Pretilt angle $\alpha$ (in degrees).

| Sample | Phase at 25°C | Alignment method: SiO evapd. at 60°C | PTFE | Polyimide (THOMSON-LCD) | SiO sputtered at 60°C | SiO sputtered at 80°C |
|---|---|---|---|---|---|---|
| ZLI-3219 | N | 0·3 | 0·7 | 5·2 | 1·5 | 1·7 |
| ZLI-4389 | N | 0·4 | 0·3 | 4·5 | — | — |
| ZLI-4518 | N | ~90 | — | 4·3 | ~90 | ~90 |
| ZLI-4801.100 | N | — | — | 2 | — | — |
| S3 | $S_A$ | 3·3 | 4·3 | 5·7 | — | — |
| K24 | $S_A$ | 0·5 | — | 5·5 | — | — |

Results show that the molecular orientation and the pretilt angle $\alpha$ are highly dependent on the liquid crystal/orientation layer couple. Figure 11 represents the measured transmission for two cells with exactly the same thickness and orientation layer (polyimide deposited by THOMSON LCD), but with two different nematic compounds. The curves obtained are very different, and the position of the symmetrical angle $\Psi_x$ changes: with ZLI-3219 *(a)* we have $\Psi_x = 17{\cdot}5°$ and so $\alpha = 5{\cdot}5°$, and with the ZLI-4801.100 *(b)* we have $\Psi_x = 4{\cdot}5°$ and so $\alpha = 1{\cdot}5°$. Figure 12 shows the measured transmission for the same nematic liquid crystal on four different alignment layers: *(a)* SiO evaporated at 60°, *(b)* SiO sputtered at 80°, *(c)* PTFE, and *(d)* THOMSON polyimide. The curves and the $\Psi_x$ positions are different and so the calculated values of $\alpha$ are quite different too. We found 0·3° for *(a)*, 1·7° for *(b)*, 0·7° for *(c)* and 5·5° for *(d)*. Results obtained on the PTFE surface are in agreement with those described by Hubert [15] who found planar anchoring with MBBA, 5CB or 7BPI aligned on PTFE layers. We also observe very different orientations on evaporated SiO layers depending on the liquid crystal used: for example, a 1000 Å thick SiO layer evaporated at 60° can induce a planar orientation with ZLI-3219 and a homeotropic alignment with ZLI-4518.

Concerning the SiO alignment layer, we changed the thickness from 100 to 2000 Å and we observed that the

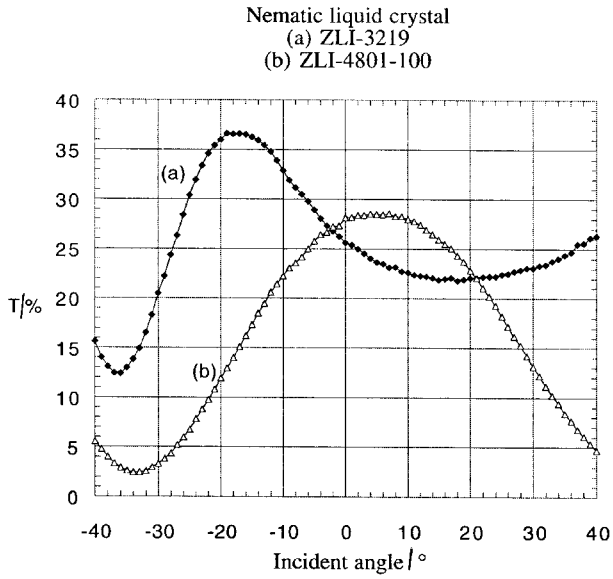


Figure 11. Measured transmission $T$ as a function of incident angle for two nematic cells with $d = 14$ μm on a polyimide layer deposited by THOMSON LCD, with two different liquid crystals: *(a)* ZLI-3219, $\Psi_x = 17{\cdot}5°$, $\alpha = 5{\cdot}5°$; *(b)* ZLI-4801.100, $\Psi_x = 4{\cdot}5°$, $\alpha = 1{\cdot}5°$.

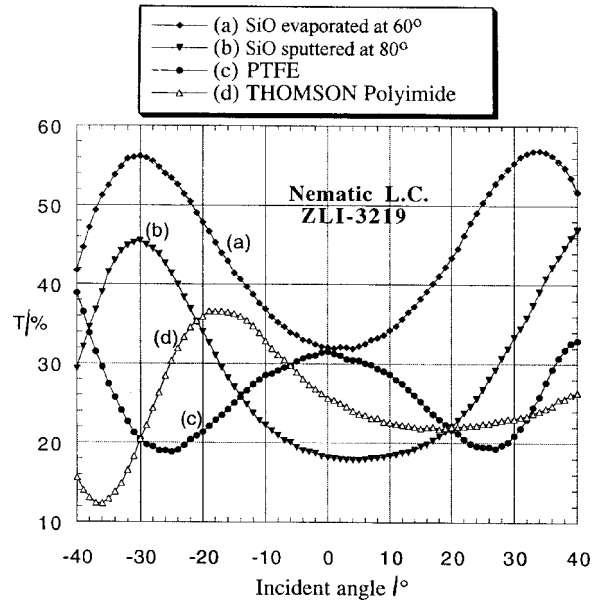


Figure 12. Measured transmission $T$ as a function of incident angle for the nematic liquid crystal ZLI-3219 on four different orientation layers: *(a)* SiO layer evaporated at 60°, $\Psi_x = 1°$, $\alpha = 0{\cdot}3°$; *(b)* SiO layer sputtered at 80°, $\Psi_x = 5{\cdot}5°$, $\alpha = 1{\cdot}7°$; *(c)* PTFE, $\Psi_x = 2°$, $\alpha = 0{\cdot}7°$; *(d)* polyimide deposited by THOMSON LCD, $\Psi_x = 17{\cdot}5°$, $\alpha = 5{\cdot}5°$.

measured pretilt angle was independent of these values, but the contrast observed through an optical microscope is better for cells with SiO layers thicker than 500 Å.

We also measured pretilt angles for the smectic A phase with K24 and S3. Figure 13 shows the transmission curves obtained for these two different liquid crystal materials, with SiO evaporated at 60°. We obtained a pretilt angle $\alpha = 0{\cdot}5°$ with K24, and $\alpha = 3{\cdot}3°$ with S3. As for the nematic phase, the results depend on the liquid crystal/orientation layer couple.

Note that all of these experimental results are highly dependent on the zone measured in the cell and the interpretation has to be linked to a systematic microscopic observation. Figure 14 shows, for example, the measured transmission for two different zones in a smectic A cell. The curve *(a)* corresponds to a well oriented zone where $\Psi_x$ can be evaluated, whereas curve *(b)* corresponds to a zone with many defects where the extremum cannot be found.

## 5. Conclusion

The optical set-up we built can be used to measure pretilt angles in parallel aligned liquid crystal cells with the same precision and reproducibility for every cell thickness value. Based on the crystal rotation method, the principle of this experimental set-up is to measure the optical transmission of a liquid crystal cell as a function of the incident light angle. Samples are parallel plate liquid crystal cells with materials in the nematic or smectic A phase, on different orientation layers. The presence of a Soleil–Bravais compensator makes precision measurements less dependent on the cell retardation. The precision obtained in the determination of the pretilt angle is 0·3°. The main result of this work is to show that the pretilt value is highly dependent on the liquid crystal/orientation layer couple chosen. In fact, we obtained pretilt values that were very different for one material on different layers and also for several materials on the same layer. More detailed results specific for every type of orientation layer and with temperature variations and phase transitions will be published later.

The crystal rotation method we used has some limitations, such as the impossibility of measuring high tilt angles (higher than 15°) generated for example by SiO evaporated at 80°.

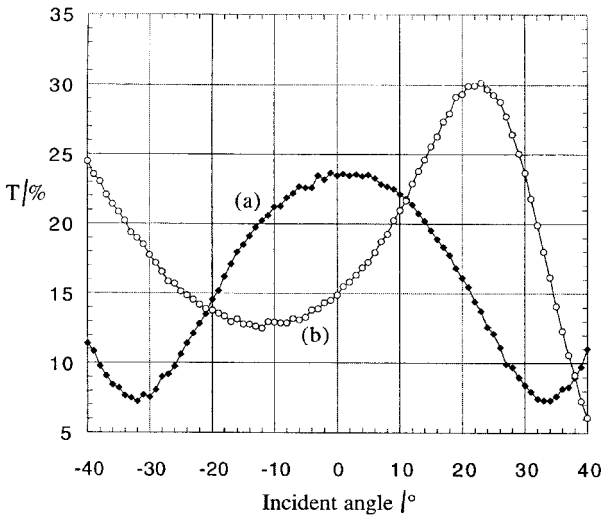


Figure 13. Measured transmission $T$ as a function of incident angle for two smectic A cells with $d = 15\,\mu m$ and SiO evaporated at 60°, for two different liquid crystals: *(a)* liquid crystal K24, $\Psi_x = 1{\cdot}5°$, $\alpha = 0{\cdot}5°$; *(b)* liquid crystal S3, $\Psi_x = 10{\cdot}5°$, $\alpha = 3{\cdot}3°$.

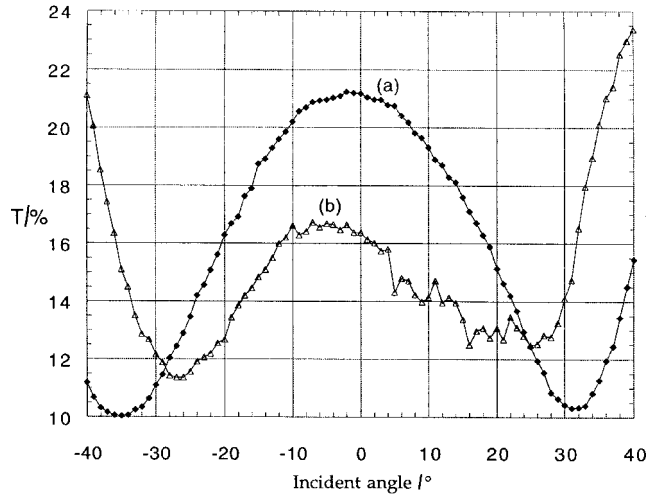


Figure 14. Measured transmission $T$ as a function of the incident angle $\Psi$ for two different zones in a smectic A cell, with the liquid crystal K24, SiO evaporated at 60°, and $d = 15\,\mu m$. For *(a)* $\Psi_x = 2°$, $\alpha = 0.°6$; for *(b)* the evaluation of $\Psi_x$ is not possible.

We gratefully acknowledge the technical assistance of J. Sarradin and Ms. A. Allegret. We are also grateful to M. Ribes and C. Llinares for helpful discussions and suggestions, and to SFIM-ODS for lending us a part of this set-up.

## References

[1] Morrissy, J. H., Crossland, W. A., and Needhan, B., 1977, *J. Phys. D,* **10,** L175.
[2] Kahn, F. J., *Mol. Cryst. liq. Cryst., 1977,* **38,** 109.
[3] Kosmowski, B. B., Becker, M. E., Cremers, R. A., and Mlynski, D. A., 1981, *Mol. Cryst. liq. Cryst.,* **72,** 17.
[4] Opara, T., Baran, J. W., and Zmija, J., 1988, *Cryst. Res. Technol.,* **23,** 1073.
[5] Lelidis, I., Gharbi, A., and Durand, G., 1992, *Mol. Cryst. liq. Cryst.,* **223,** 263.
[6] Becker, M. E., 1996, *SID*, **2**.
[7] Baur, G., Wittwer, V., and Berreman, D. W., 1976, *Phys. Lett.,* **56A,** 142.

[8] SCHEFFER, T. J., and NEHRING, J., 1977, *J. appl. Phys.,* **48,** 1783.
[9] FRANÇON, M., 1956, *Handbuch der Physik,* Vol. XXIV, edited by S. Flügge (Berlin: Springer), 441.
[10] BORN, M., and WOLF, E., 1964, *Principles of Optics* (Oxford: Pergamon Press).
[11] JANNING, J. L., 1972, *Appl. Phys. Lett.,* **21,** 173.
[12] MONKADE, M., BOIX, M., and DURAND, G., 1988, *Europhys. Lett.,* **5,** 697.
[13] MOTOHIRO, T., and TAGA, Y., 1990, *Thin Solid Films,* **185,** 137.
[14] WITTMANN, J-C., and SMITH, P., 1991, *Nature,* **352,** 414.
[15] HUBERT, P., DREYFUS, H., GUILLON, D., and GALERNE, Y., 1995, *J. Phys. II,* **5,** 1371.